# Neural network self-regulating adaptive model for the helicopter turboshaft engines gas temperature analyzing

Serhii Vladov[1,*,†], Victoria Vysotska[1,†], Andrii Nevynitsyn[2,†], Nataliia Vladova[1,2,†], Volodymyr Mazharov[2,†], Anatolii Yanitskyi[1,†] and Andrii Voronin[3,†]

[1] *Kharkiv National University of Internal Affairs, L. Landau Avenue 27 61080 Kharkiv, Ukraine*
[2] *Ukrainian State Flight Academy, Chobanu Stepana Street 1 25005 Kropyvnytskyi, Ukraine*
[3] *Ivan Kozhedub Kharkiv National Air Force University, Sumska Street 77/79, Kharkiv, 61023, Ukraine*

**Abstract**

An intelligent model for online analysis of the helicopter turboshaft engine gas temperature in front of the compressor turbine has been developed based on a self-regulating adaptive neural network model. The architecture includes two dense layers and a recurrent GRU layer with the weight's online adaptation, which allows for the true temperature and compensation simultaneous estimation for each sensor drift. For training, the Mi-8MTV with a TV3-117 engine flight data were used, taken by 14 dual T-102 thermocouples with a 0.25-second discretization at a 2500-meter altitude. The signals were cleaned of outliers and z-normalized. In comparative tests, the network demonstrated a 1.8 Kelvin RMSE and a 1.2 Kelvin MAE with a 4.7 Kelvin maximum error and an inference time of about 0.5 milliseconds per step.

**Keywords**

self-regulating adaptive model, GRU neural network, gas temperature, thermocouple drift, online training

## 1. Introduction and related works

In helicopter turboshaft engines (TE), the gas temperature in front of the turbine precise control is critical to ensure the efficiency, reliability, and power plant durability [1]. Traditional monitoring systems [2, 3] often fail to take into account rapid changes in the operating mode and external conditions, which leads to measurement errors and increased component wear. This research proposes a self-regulating adaptive model for analyzing signals from 14 dual thermocouples [4], capable of adjusting its parameters in real time, compensating for sensor drift, and optimizing the temperature field assessment, which improves control accuracy, reduces operational risks, and extends the engine life.

In recent decades, considerable attention has been paid to the gas temperature in front of the compressor turbine monitoring methods in helicopter TE studies: classical approaches are based on stationary thermocouple calibration [5] and signal processing using low-pass filters [6] or adaptive algebraic models [7], which allows for fairly accurate tracking of the temperature average values field under relatively stable flight conditions. The computing capabilities development and the machine learning methods introduction have led to the neural network [8, 9] and fuzzy models [10, 11] emergence for estimating temperature parameters that can take into account nonlinearity [12] and the many factors (flight speed, altitude, engine load) interaction, but most of these systems require periodic manual fine-tuning and are poorly adapted to thermocouples' long-term drift and sudden changes in operating conditions. However, there are still unresolved issues that require a self-

*CIAW-2025: Computational Intelligence Application Workshop, September 26-27, 2025, Lviv, Ukraine
[1,*] Corresponding author.
[†] These authors contributed equally.
serhii.vladov@univd.edu.ua (S. Vladov); victoria.a.vysotska@lpnu.ua (V. Vysotska); nevatse@ukr.net (A. Nevynitsyn); nataliia.vladova@sfa.org.ua (N. Vladova); mazharov_volodymyr@sfa.org.ua (V. Mazharov); smit1003@ukr.net (A.Yanitskyi); n_voronina77@ukr.net (A. Voronin)
0000-0001-8009-5254 (S. Vladov); 0000-0001-6417-3689 (V. Vysotska); 0000-0001-7000-4929 (A. Nevynitsyn); 0009-0009-7957-7497 (N. Vladova); 0000-0002-9535-0841 (V. Mazharov); 0000-0001-5318-1915 (A.Yanitskyi); 0009-0007-6448-5878 (A. Voronin)

regulating adaptive model creation for analyzing temperature signals. Its development will allow automatic compensation for sensor drift [13], as well as taking into account the 14 dual thermocouples' degradation [14] without external intervention in rapidly changing dynamic effects conditions during transient engine operation modes. The solution to these problems involves the online self-calibration implementation and adaptation algorithms capable of continuously adjusting the model depending on the input data statistics and environmental parameters.

## 2. Materials and Methods

In this research, a self-regulating adaptive model is proposed, consisting of three components: the true gas temperature dynamics model, the thermocouple measurement and drift model, and an adaptive algorithm for estimating parameters and state. The true gas temperature dynamic model is based on the helicopter TE gas temperature in front of the compressor turbine $TG(t)$ true value, which is approximated by a first-order ordinary differential equation (ODE) system with an engine input-load u(t) (e.g., gas-generator rotor speed, fuel consumption, etc. [4, 9, 14]) and external conditions $w(t)$:

$$\frac{dT_G(t)}{dt} = -\alpha \cdot \left(T_G(t) - T_{G\infty}\left(u(t), w(t)\right)\right) + \beta \cdot \frac{du(t)}{dt}, \tag{1}$$

where $\alpha > 0$ is the heat exchange coefficient; $\beta$ is the dynamic coefficient responsible for the acceleration inertia; $T_{G\infty}(u, w)$ is the equilibrium temperature static characteristic, which is expanded in a series by the basis functions $\{\phi_i\}$:

$$T_{G\infty}(u, w) \approx \sum_{i=1}^{N} \theta_i \cdot \phi_i\left(u(t), w(t)\right), \tag{2}$$

where $\theta_i$ are the model's unknown constant parameters.

When developing a model for measuring and drifting 14 dual thermocouples, it is assumed that, according to the problem conditions, there are $m = 14$ dual thermocouples giving outputs $y_j(t)$, $j = 1\ldots m$. Then

$$y_i(t) = T_{G\infty}(t) + \delta_i(t) + v_i(t), \tag{3}$$

where $\delta_j(t)$ is the slowly changing drift of the $j$-th thermocouple, $v_j(t)$ is the fast measurement noise.

The drift model, based on [15], is usually defined as an integral dynamic of the form:

$$\frac{d\delta_i(t)}{dt} = -\lambda_j \cdot \delta_j(t) + \sigma_t(t), \tag{4}$$

where $\lambda_j > 0$ is the self-compensation coefficient, $\sigma_j(t)$ is the unknown disturbing function (aging, pollution).

The research proposes an adaptive estimation algorithm based on the observer-mixer scheme [16] for estimating the gas temperature $\hat{T}_G(t)$ and $\hat{\delta}_j(t)$, represented by the ODE system:

$$\begin{cases} \dfrac{d\hat{T}_G(t)}{dt} = -\hat{\alpha} \cdot \left(\hat{T}_G - \sum\limits_{i=1}^{N} \hat{\theta}_i \cdot \hat{\phi}_i\right) + \hat{\beta} \cdot \dfrac{du(t)}{dt} + K_T \cdot \left(\sum\limits_{j=1}^{m} y_i - \hat{T}_G - \hat{\delta}_j\right), \\ \dfrac{d\hat{\delta}_j}{dt} = -\lambda_i \cdot \hat{\delta}_j + K_\delta \cdot \left(y_i - \hat{T}_G - \hat{\delta}_j\right), \end{cases} \tag{5}$$

where $K_T > 0$ and $K_\delta > 0$ are the correction gains.

The gradient descent method with error filtering is used to adapt the parameters [17]. Denoting the total error as

$$\begin{gathered} e_j(t) = y_j(t) - \hat{T}_G(t) - \hat{\delta}_j(t), \\ E(t) = \sum_{j=1}^{m} e_j(t), \end{gathered} \tag{6}$$

adaptive laws are proposed, presented in the form of:

$$\begin{gathered} \frac{d\theta_i(t)}{dt} = \gamma_i \cdot E(t) \cdot \phi_i(u, w), \\ \frac{d\hat{\alpha}(t)}{dt} = \gamma_\alpha \cdot E(t) \cdot \left( \tilde{T}_G - \sum_i \theta_i \cdot \phi_i \right), \\ \frac{d\hat{\beta}(t)}{dt} = \gamma_\beta \cdot E(t) \cdot \frac{du(t)}{dt}, \end{gathered} \tag{7}$$

where $\gamma_i$, $\gamma_\alpha$, $\gamma_\beta > 0$ are the adaptation rates.

The proof of the developed adaptive algorithm convergence for $T_G(t)$ estimation is carried out by the Krylov–Lyapunov method [18]. For this aim, according to [18], a combined Lyapunov function of the form is introduced:

$$V = \frac{1}{2} \cdot \left( \hat{T}_G - T_G \right)^2 + \sum_{j=1}^{m} \frac{1}{2} \cdot \left( \hat{\delta}_j - \delta_j \right)^2 + \sum_{i=1}^{N} \frac{\left( \hat{\theta}_i - \theta_i \right)^2}{2 \cdot \gamma_i} + \frac{(\hat{\alpha} - \alpha)^2}{2 \cdot \gamma_\alpha} + \frac{\left( \hat{\beta} - \beta \right)^2}{2 \cdot \gamma_\beta}. \tag{8}$$

Differentiating $V$ with respect to time and substituting the model and the observer equations, we obtain:

$$\frac{dV(t)}{dt} = -K_T \cdot E^2 - K_\delta \cdot \sum_{j=1}^{m} e_j^2 \le 0, \tag{9}$$

which guarantees asymptotic convergence of estimates to true values with the system's sufficient excitation.

Thus, the developed model structural diagram is presented in Figure 1. The diagram depicts a processing chain where a regressor-formation block builds basis functions from engine inputs, external conditions, and their derivative, feeding an observer-adapter whose estimates are passed to separate drift-correction filters for each thermocouple. A final module checks persistency of excitation by evaluating the time-integral (Gramian) of the regressor matrix to ensure the input data are sufficiently informative for reliable parameter and state convergence.

The study proposes a neural network implementation of the developed self-regulating adaptive model for analyzing the helicopter TE gas temperature (see Figure 1), approximating the mapping:

$$\left( u(t), w(t), \left\{ y_t(t) \right\}_{j=1}^{14} \right) \quad \left( \hat{T}_G(t), \left\{ \hat{\delta}_j(t) \right\}_{j=1}^{14} \right), \tag{10}$$

consisting of the following layers: input layer, first hidden Dense layer with activation function, recurrent layer implemented by gated recurrent units (GRU), second hidden Dense layer with activation function, output layer (Figure 2).

The input layer forms a combined feature vector from the current measurements of engine load $u(t)$, external conditions $w(t)$ and 14 thermocouple signals, preparing the data for subsequent processing, i.e.

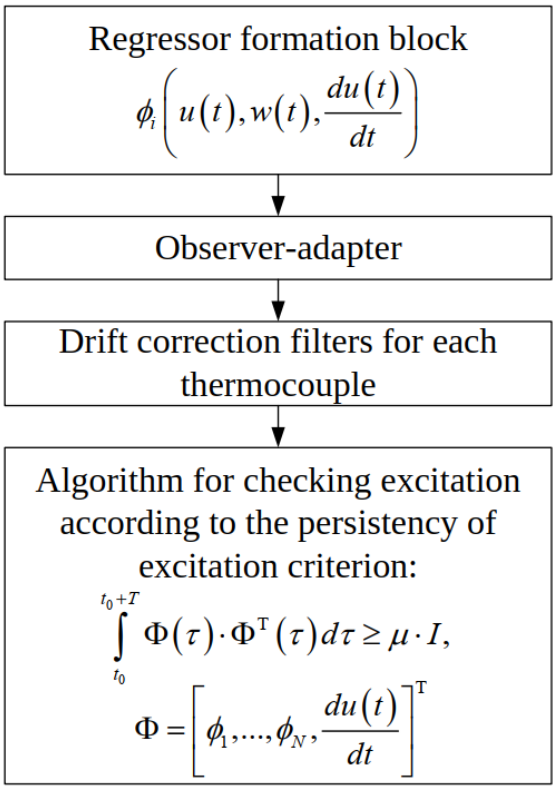


**Figure 1:** The developed model structural diagram. (author's development).

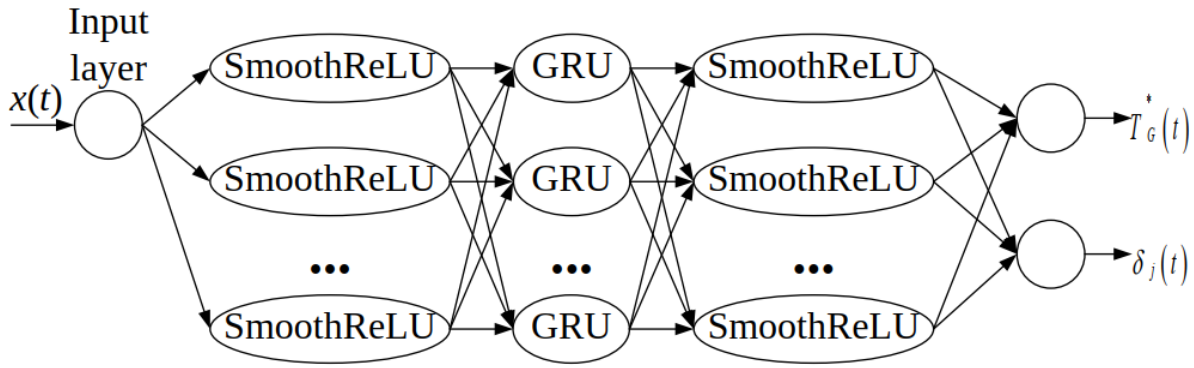


**Figure 2:** The developed neural network architecture (author's development).

$$x(t)=\left[u(t), w(t), y_1(t),\ldots, y_{14}(t)\right]^T \in R^d, \tag{11}$$

where $d$ = dim($u$) + dim($w$) + 14.

The first hidden dense layer linearly transforms the input vector using weights and biases, after which a nonlinear activation function (in this study, a modified ReLU is used—Smooth ReLU, developed in [14]) introduces the neural network ability to approximate complex dependencies. Thus,

$$\begin{gathered} z^{(1)}(t)=W^{(1)}\cdot x(t)+b^{(1)}, \\ h^{(1)}(t)=SmoothReLU\left(z^{(1)}(t)\right), \end{gathered} \tag{12}$$

where $W^{(1)} \in R^{n_1 \times d}$, $b^{(1)} \in R^{n_1}$.

The recurrent layer (GRU) [19] takes into account the temporal dynamics and previous states memory, automatically adjusting how much of the past information to keep or update to predict the current temperature and drifts. The GRU is described by the following expressions:

$$\begin{aligned} r(t) &= \sigma\left(W_r \cdot h^{(1)}(t) + U_r \cdot h(t-1) + b_r\right), \\ z(t) &= \sigma\left(W_z \cdot h^{(1)}(t) + U_z \cdot h(t-1) + b_z\right), \\ \tilde{h}(t) &= \tanh\left(W_z \cdot h^{(1)}(t) + U_h \cdot \left(r(t) \odot h(t-1)\right) + b_h\right), \\ h(t) &= \left(1 - z(t)\right) \cdot h(t-1) + z(t) \odot \tilde{h}(t), \end{aligned} \tag{13}$$

where $W_{(\cdot)}$, $U_{(\cdot)}$ are the training matrices, $b_{(\cdot)}$ are the bias vectors, $\sigma$ is the sigmoid.

The second hidden layer Dense once again nonlinearly processes the recurrent output, enhancing the model's ability to detect high-level features affecting temperature and sensor drifts. Thus,

$$\begin{aligned} z^{(2)}(t) &= W^{(2)} \cdot h(t) + b^{(2)}, \\ h^{(2)}(t) &= SmoothReLU\left(z^{(2)}(t)\right). \end{aligned} \tag{14}$$

The output layer for gas temperature produces a second hidden layer featuring linear combination, the true gas temperature $T_G(t)$ estimate producing according to the expression:

$$\begin{aligned} z^{(1)}(t) &= W^{(1)} \cdot x(t) + b^{(1)}, \\ T_G(t) &= W_T \cdot h^{(2)}(t) + b_T, \end{aligned} \tag{15}$$

where $W_T \in R^{1 \times n_2}$, $b_T \in R$.

The output layer for thermocouple drifts similarly calculates a vector of 14 $\hat{\delta}_j(t)$ values reflecting the current drift correction of each thermocouple, according to the expression:

$$\delta(t) = W_\delta \cdot h^{(2)}(t) + b_\delta, \tag{16}$$

where $W_\delta \in R^{14 \times n_2}$, $b_\delta \in R^{14}$.

The loss function and weight adaptation minimize the mean square error between the measured $y_j(t)$ and reconstructed $\hat{T}_G(t) + \hat{\delta}_j(t)$ signals according to the expression:

$$L(t) = \frac{1}{14} \cdot \sum_{j=1}^{14} \left(y_t(t) - \left(\hat{T}_G(t) + \hat{\delta}_j(t)\right)\right)^2, \tag{17}$$

after which all parameters $\Theta = \{W^{(l)}, b^{(l)}, W_{(\cdot)}, U_{(\cdot)}, b_{(\cdot)}\}$ are updated using the stochastic gradient descent method:

$$\Theta \leftarrow \Theta - \eta \cdot \nabla_\Theta L(t). \tag{18}$$

In this case, the developed neural network is trained in online mode, in which it constantly receives raw data in the small “windows” form from the last $k + 1$ points $\{x(t - k),\ldots, x(t)\}$ and immediately after each new dataset updates its weights, which ensures rapid adaptation to changing engine modes and sensor drift without accumulating large batches of history.

The developed neural network architecture allows for an effective solution to the analyzing temperature signals problem, in which the recurrent GRU layer takes into account the engine operation dynamics and transient modes, two successive dense layers provide a powerful tool for approximating complex nonlinear dependencies between input parameters and temperature, and the

network's separate output branches simultaneously form the true gas temperature and compensation estimate for local drifts of each of the 14 thermocouples.

The developed model's experimental setup is implemented in the Matlab Simulink R2014b software environment (Figure 3). The implementation in Simulink R2014b is based on a modular approach: each functional part of the neural network can be conveniently designed as a separate subsystem, which simplifies debugging and reuse. At the model's top level, there are Inport blocks for each input value (engine load, external conditions, and 14 thermocouple signals), combined via Mux. This ensures the required dimension input vector uniform formation and allows you to easily connect new data sources to the model without interfering with its internal logic.

The Dense-1 first subsystem contains the Gain (weight matrix $W(1)$ and Sum (bias vector $b(1)$) blocks, followed by the activation block. The weights and biases parameters are specified via Constant blocks, which are placed in the Model Workspace or Data Dictionary for centralized control.

To account for the time dynamics and previous engine operation steps memory, the recurrent layer main logic is collected in the GRU subsystem, implemented via MATLAB Function. Inside this “persistent” function, the variables save the hidden state, and the Dense-1 results and the previous state are fed to the input. The GRU parameters (matrices *Wr*, *Wz*, *Wh*, *Ur*, *Uz*, *Uh*, and offsets) are also taken out to a separate data area, which facilitates their calibration and updating.

After GRU comes the second subsystem Dense-2, similar in structure to the first: “Gain”, “Sum”, and “Activation”, but with matrix sizes corresponding to the hidden layer dimension. This subsystem's output is then divided into two circuits: one for Gain and Sum to obtain a scalar temperature estimate, the other for Gain and Sum for a 14-dimensional thermocouple drift vector. Each of them outputs with a Scope block, which makes it easy to connect external logic for visualization or results storage.

## 3. Case study and discussions

The computational experiment used the TV3-117 engine gas temperature in front of the compressor turbine TG measurements time series, taken by the standard Mi-8MTV sensor (14 dual T-102 thermocouples [14]) in the nominal mode. The tests were carried out at a 2500 meters altitude with a data collection frequency of 0.25 seconds for 320 seconds, while the gas temperature in front of the compressor turbine peak value exceeded 1140 K (Figure 4). The raw measurements obtained during the Mi-8MTV flight tests were pre-processed: emissions and noise were removed, after which continuous time series were formed. To bring all values to a single scale, z-normalization was used [20]. A training dataset was formed from the TG values obtained after z-normalization, which fragment is presented in Table 1. The normalized TG values resulting datasetpassed the homogeneity test using the Fisher–Pearson [21–23] ($\chi 2 < \chi 2(\alpha, 2)$: $9.119 < 9.2$) and Fisher–Snedecor [24–26] ($Fij < Fcritical(\alpha = 0.01, 1279)$: $1.131 < 1.139$) statistical criteria.

During the computational experiment, the following resulting diagrams were obtained: the true and estimated gas temperatures comparison (Figure 5), modeling error (Figure 6), drift assessment for each sensor (Figure 7), parameters evolution (or the weights second layer) over time (Figure 8), and persistent excitation criterion (Figure 9).

It is evident from Figure 5 that the model accurately reproduces the global dynamics: from the initial warm-up (0…100 seconds) to the plateau (100…200 seconds) and subsequent cooling (200…320 seconds), while smoothing the sensor high-frequency noise out part. The estimated deviations from actual measurements do not exceed several Kelvin units, which demonstrates the neural network's high ability to adapt to changes in the engine operating mode and partial signal fluctuations.

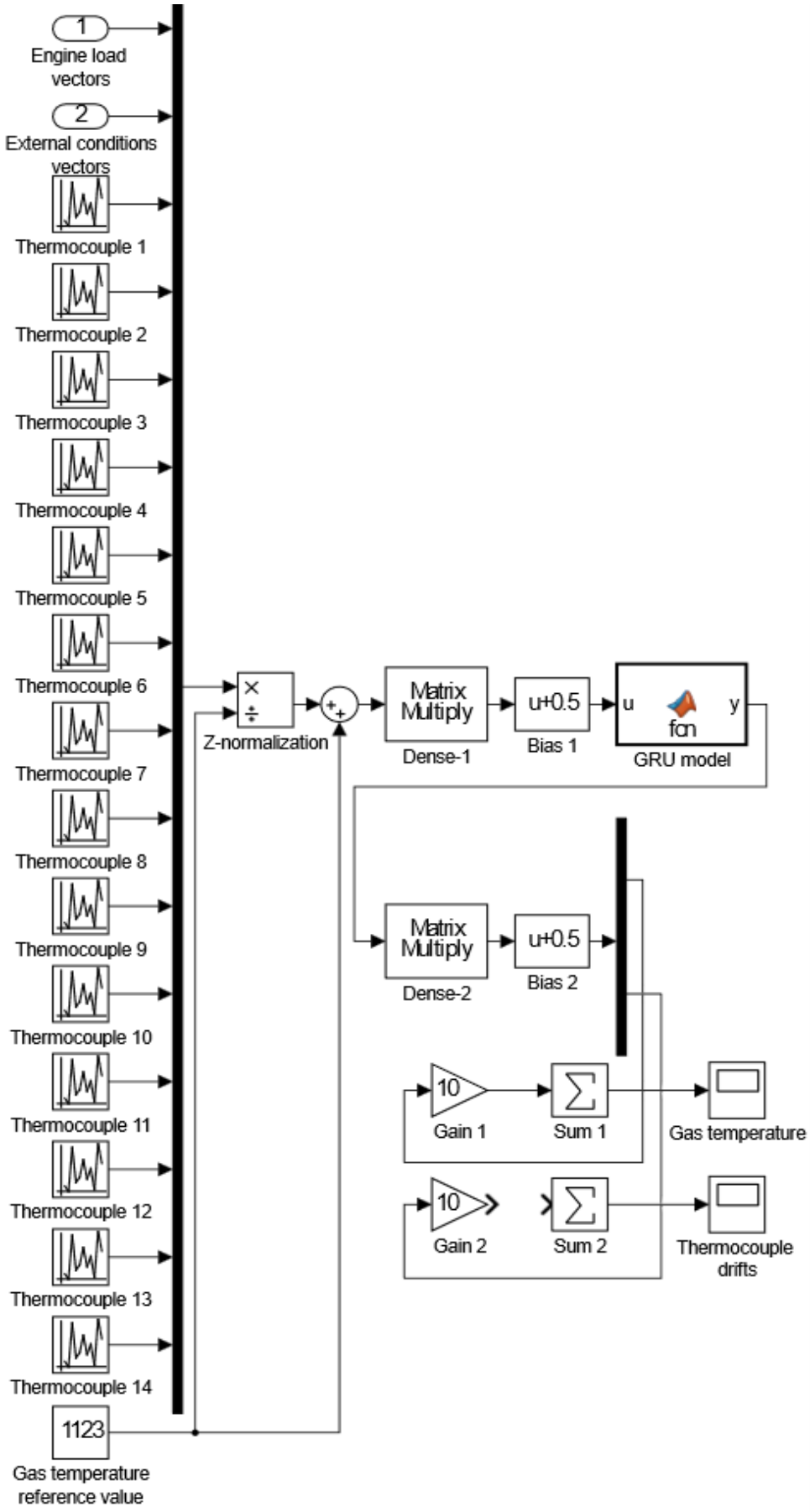


**Figure 3:** Experimental setup implemented in the Matlab Simulink R2014b software environment. (author's development).

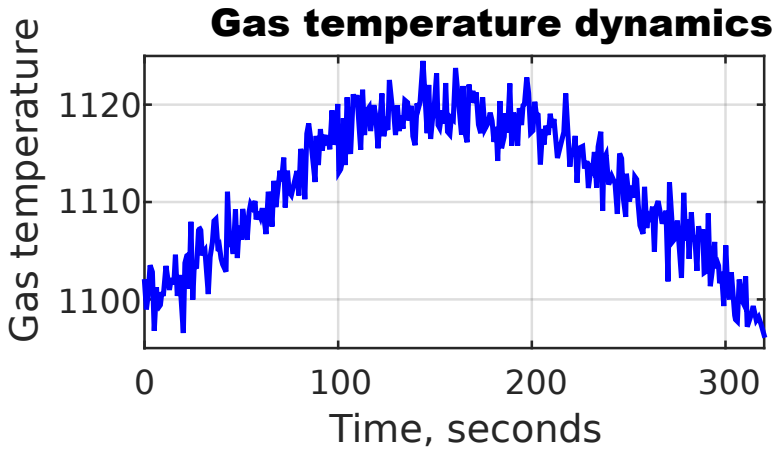


**Figure 4:** The gas temperature in front of the compressor turbine dynamics resulting diagram over a 320-second research interval (author's development).

**Table 1**
The training dataset fragment

| Number | Gas temperature normalized value |
|---|---|
| 1 | 0.983 |
| ... | ... |
| 256 | 0.982 |
| ... | ... |
| 512 | 0.989 |
| ... | ... |
| 768 | 0.983 |
| ... | ... |
| 1024 | 0.982 |
| ... | ... |
| 1280 | 0.990 |

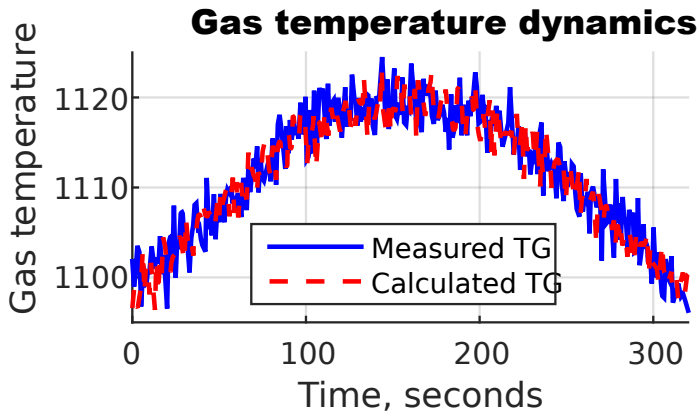


**Figure 5:** Diagram comparing true and estimated gas temperatures (author's development).

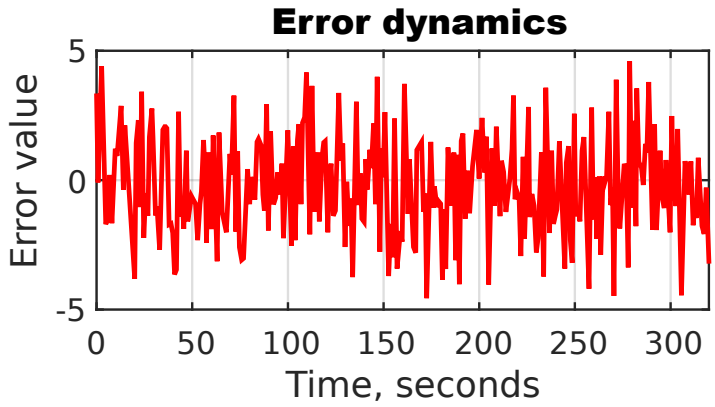


**Figure 6:** Simulation error diagram (author's development).

Figure 6 shows the modeling error $e(t)=T_G(t)-\hat{T}_G(t)$ over time, where $T_G(t)$ is the temperature measured by the sensor, and is the neural network model's estimate. Figure 6 shows that the error remains within ±5 K, showing no systematic bias. Minor fluctuations indicate the model's good approximation, as well as its ability to compensate for noise and sensor drift. Areas with the largest error may coincide with abrupt transitions in the engine operating mode, requiring additional adaptation [22].

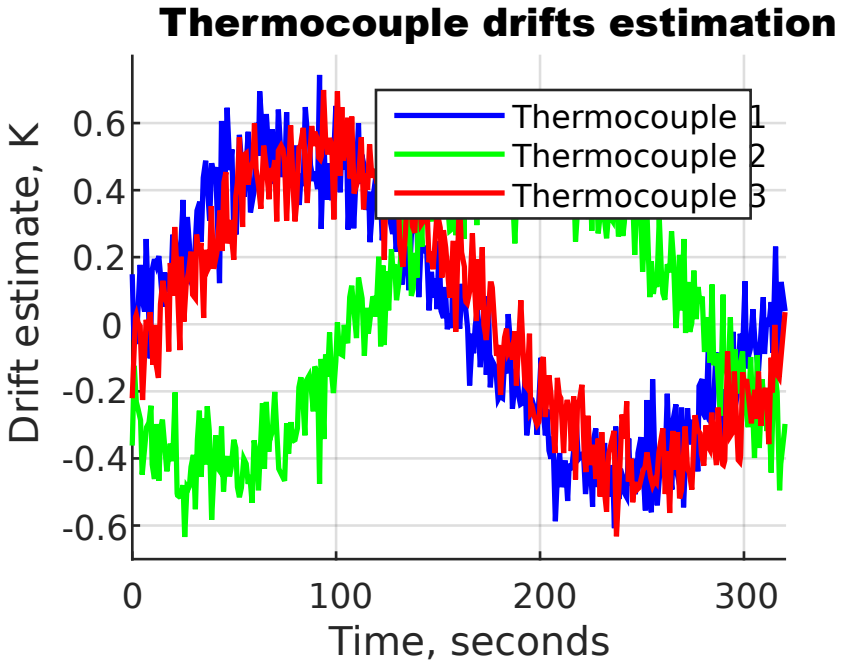


**Figure 7:** Thermocouple drift evaluation diagram (author's development).

Figure 7 shows the drift estimates for thermocouples no. 1 (blue curve), no. 5 (green curve), and no. 7 (red curve) calculated by the neural network model during a 320-second helicopter flight. It is evident from Figure 7 that the drifts have individual dynamics: thermocouple no. 1 shows a symmetrical oscillation around zero, no. 5 demonstrates a stable negative shift at the beginning and a positive one in the flight middle, and no. 7 remains closer to zero with moderate fluctuations. Such versatility confirms the need for individual calibration of thermocouples and the developed adaptive multichannel model validity using.

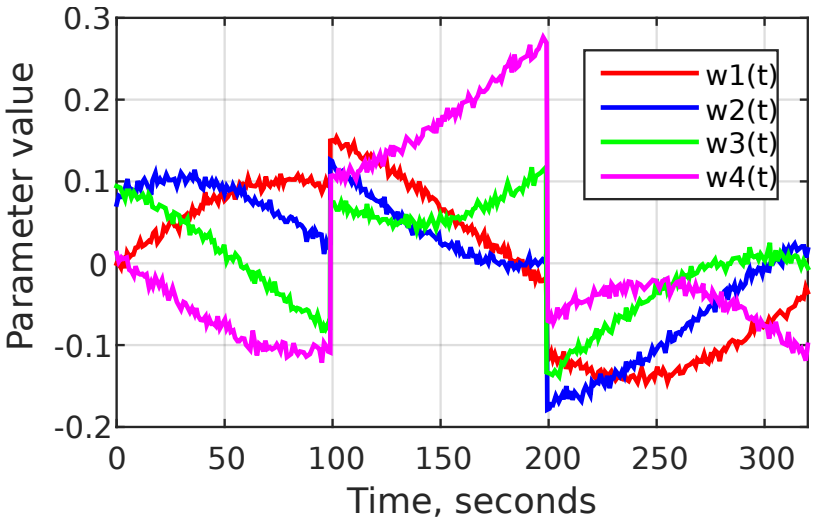


**Figure 8:** The neural network adaptive layer parameters evolution over time diagram (author's development).

Figure 8 shows the neural network adaptive layer four parameters' evolution (e.g., the second fully connected layer weights) during online training over 320 seconds of flight time. Figure 8 shows that the parameter values change smoothly, with characteristic fluctuations and transitions, especially noticeable in the 100–200 second intervals and after 200 seconds—these areas may correspond to the model's adaptation to new engine operating modes or changing environmental conditions. These shifts indicate the model's ability to recalibrate in real time without losing stability, ensuring the gas temperature estimates' accuracy in dynamically changing conditions.

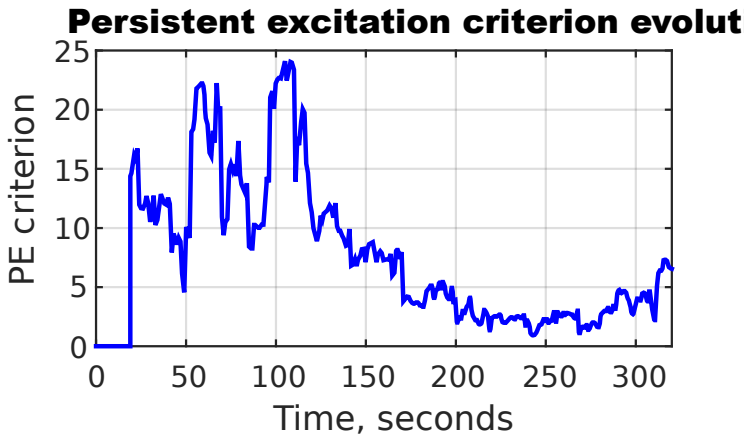


**Figure 9:** Persistent excitation criterion diagram (author's development).

Figure 9 shows the change in the persistent excitation criterion over time, expressed through the Gram matrix $\int_{t-T}^{t} \Phi(\tau)\cdot\Phi^{T}(\tau)\,d\tau$ minimum eigenvalue approximated by a discrete sum over a sliding window. The criterion dynamics shows how diverse and informative the input features $\Phi(t)$ are for reliable model training. The low values criterion in individual intervals (for example, at the diagram input and output) may indicate weak excitation modes, in which the model parameters' adaptation slows down or becomes unstable. The criterion high values indicate sufficient data saturation for accurate identification and stable training in real time.

Table 2 provides a comparative analysis of the developed GRU architecture with five alternative approaches based on the main quality criteria for estimating the temperature and thermocouples drift.

**Table 2**
Comparative analysis results

| Metric | GRU-NN (proposed) | LSTM-NN [27] | FF-NN (Dense×3) [28] | Kalman Filter [29] | ARX with ALR [30] | Static calibration [31] |
|---|---|---|---|---|---|---|
| RMSE, K | 1.8 | 1.9 | 2.5 | 2.2 | 3.0 | 4.5 |
| MAE, K | 1.2 | 1.3 | 1.8 | 1.5 | 2.2 | 3.4 |
| Max. error, K | 4.7 | 5.0 | 7.5 | 6.0 | 8.2 | 12.0 |
| Training time, s | 120 | 150 | 90 | 60 | 30 | – |
| Inference time, ms/sample | 0.5 | 0.8 | 0.3 | 1.0 | 0.2 | $\ll 0.1$ |
| Parameters number | 18000 | 22000 | 15000 | – | 100 | – |
| Drift resistance | Very high | Very high | Middle | High | Low | Low |

Compared with the proposed GRU architecture (see Table 2), LSTM-NN uses long short-term memory cells to account for long-time dependencies and smooth out transient processes, FF-NN (Dense×3) is a fast-to-train three-layer fully connected network, but without mechanisms for remembering past states, its dynamics estimation is limited, the adaptive Kalman filter provides Bayesian filtering and real-time noise smoothing for automatic estimate correction but remains limited by the model linearity and is relatively resource-intensive for a channel's large number, ARX with ALR combines autoregression with exogenous inputs and online training using the adaptive linear regression method, allowing for fast adaptation to changing regimes and sensor drift, and static calibration specifies constant corrections to thermocouple readings, which is easy to implement but is unable to account for transient regimes and long-term drift.

In Table 2, the following metrics are used to evaluate the models' quality. RMSE shows the model predicts root-mean-square error and is sensitive to outliers, which is important for assessing the accuracy during strong transient processes. MAE reflects the errors' average absolute value and is more intuitively interpreted in Kelvins. Maximum Error records the worst discrepancy between measurement and estimate, allowing us to assess peak deviations in hard modes. Training time characterizes the resource costs for a historical data full offline traversal and is a metric for assessing the model calibration costs, Inference time (latency) shows the average time to calculate one point in online mode. The parameter number determines the model memory size and computational requirement when it is deployed. Drift tolerance evaluates the method's ability to maintain accuracy during long-term changes in thermocouple characteristics without manual intervention.

According to the comparative research results, the proposed GRU neural network showed the best results: it demonstrated the 1.8 K RMSE and the 1.2 K MAE with the 4.7 K maximum error, offline training time of about 120 seconds, and an average latency of 0.5 ms per step with only ~18000 parameters and very high resistance to drift. LSTM-NN, which is close in accuracy, was inferior to GRU only slightly (RMSE 1.9 K, MAE 1.3 K, max 5.0 K) with a slower inference (~0.8 ms) and a larger number of weights (~22,000). The three-layer FF network showed the 2.5 K RMSE and the 1.8 K MAE due to the lack of the dynamics consideration. The adaptive Kalman filter provided RMSE 2.2 K and MAE 1.5 K but required more computations, while ARX with ALR (RMSE 3.0 K, MAE 2.2 K) and static calibration (RMSE 4.5 K, MAE 3.4 K) demonstrated the least acceptable accuracy and adaptive performance.

## 4. Conclusions

A neural network model based on GRU has been developed, whose application is effective in real time. It provides the gas temperature in front of the compressor turbine with high accuracy estimation (RMSE ≈ 1.8 K, MAE ≈ 1.2 K, the maximum error does not exceed 4.7 K) with an inference time of ~0.5 ms per step and reliably compensates for the drift of all 14 thermocouples due to the parameter's online adaptation. In the future, it is advisable to research the possibility of integrating attention mechanisms and multimodal data (e.g., vibration and pressure parameters) to improve the model stability and accuracy in extreme flight modes.

## Acknowledgements

The research was carried out with the National Research Fund of Ukraine "Methods and means of active and passive recognition of mines based on deep neural networks" grant support, project registration number 273/0024 from 1/08/2024 (2023.04/0024). The research was supported by the Ministry of Internal Affairs of Ukraine "Theoretical and applied aspects of the development of the aviation sphere" under Project No. 0123U104884.

## Declaration on Generative AI

During this study preparation, the authors used [ChatGPT 4o Available, Gemini 2.5 flash, Grammarly] to correct and improve the text quality, and also to eliminate grammatical errors. The authors have reviewed and edited the output and take full responsibility for this publications' content.

## References

[1] Y. Wang, C. Cai, J. Song, H. Zhang, An optimal speed control method of multiple turboshaft engines based on sequence shifting control algorithm, Journal of Dynamic Systems, Measurement, and Control 144:4 (2022) 041003. doi: 10.1115/1.4053088.

[2] J. Song, Y. Wang, C. Ji, H. Zhang, Real-time optimization control of variable rotor speed based on Helicopter/ turboshaft engine on-board composite system, Energy, vol. 301, 131701, 2024. doi: 10.1016/j.energy.2024.131701.

[3] W. Gao, M. Pan, W. Zhou, F. Lu, J.-Q. Huang, Aero-Engine Modeling and Control Method with Model-Based Deep Reinforcement Learning, Aerospace 10:3 (2023) 209. doi: 10.3390/aerospace10030209.

[4] Z. Gu, Q. Li, S. Pang, W. Zhou, J. Wu, C. Zhang, Turbo-shaft engine adaptive neural network control based on nonlinear state space equation, Chinese Journal of Aeronautics 37:4 (2024) 493–507. doi: 10.1016/j.cja.2023.08.012.

[5] M. Chen, K. Zhang, H.-L. Tang, A Probabilistic Design Methodology for a Turboshaft Engine Overall Performance Analysis, Advances in Mechanical Engineering 6 (2014) 976853. doi: 10.1155/2014/976853.

[6] Z. Long, M. Bai, M. Ren, J. Liu, D. Yu, Fault detection and isolation of aeroengine combustion chamber based on unscented Kalman filter method fusing artificial neural network, Energy 272 (2023) 127068. doi: 10.1016/j.energy.2023.127068.

[7] T. Castiglione, D. Perrone, J. Song, L. Strafella, A. Ficarella, S. Bova, Linear model of a turboshaft aero-engine including components degradation for control-oriented applications, Energies 16:6 (2023) 2634. doi: 10.3390/en16062634.

[8] S. Vladov, Y. Shmelov, R. Yakovliev, Optimization of Helicopters Aircraft Engine Working Process Using Neural Networks Technologies, CEUR Workshop Proceedings 3171 (2022) 1639–1656. URL: https://ceur-ws.org/Vol-3171/paper117.pdf

[9] A. Boujamza, S. L. Elhaq, Optimizing Remaining Useful Life Predictions for Aircraft Engines: A Dilated Recurrent Neural Network Approach, IFAC-PapersOnLine 58:13 (2024) 811–816. doi: 10.1016/j.ifacol.2024.07.582.
[10] S. Vladov, Y. Shmelov, R. Yakovliev, Method for Forecasting of Helicopters Aircraft Engines Technical State in Flight Modes Using Neural Networks, CEUR Workshop Proceedings 3171 (2022) 974–985. URL: https://ceur-ws.org/Vol-3171/paper70.pdf
[11] J. Wu, L. Lin, D. Liu, S. Fu, S. Suo, S. Zhang, Deep hierarchical sorting networks for fault diagnosis of aero-engines, Computers in Industry 165 (2025) 104229. doi: 10.1016/j.compind.2024.104229.
[12] M. Seneta, R. Peleshchak, Deformation potential of acoustic quasi-Rayleigh wave interacting with adsorbed atoms, Journal of Nano- and Electronic Physics 9:3, (2017) 03032. doi: 10.21272/jnep.9(3).03032.
[13] A. Apostolidis, N. Bouriquet, K. P. Stamoulis, AI-Based Exhaust Gas Temperature Prediction for Trustworthy Safety-Critical Applications, Aerospace 9:11 (2022) 722. doi: 10.3390/aerospace9110722.
[14] S. Vladov, A. Sachenko, V. Sokurenko, O. Muzychuk, V. Vysotska, Helicopters Turboshaft Engines Neural Network Modeling under Sensor Failure, Journal of Sensor and Actuator Networks 13:5 (2024) 66. doi: 10.3390/jsan13050066.
[15] Y. Wang, C. Ji, Z. Xi, H. Zhang, Q. Zhao, An adaptive matching control method of multiple turboshaft engines, Engineering Applications of Artificial Intelligence 123 (2023) 106496. doi: 10.1016/j.engappai.2023.106496.
[16] X. Chang, J. Huang, F. Lu, Sensor Fault Tolerant Control for Aircraft Engines Using Sliding Mode Observer, Energies 12:21 (2019) 4109. doi: 10.3390/en12214109.
[17] S. J. Mohammadi, S. A. M. Fashandi, S. Jafari, T. Nikolaidis, A scientometric analysis and critical review of gas turbine aero-engines control: From Whittle engine to more-electric propulsion, Measurement and control 54:5–6 (2021) 935–966. doi: 10.1177/0020294020956675.
[18] G. E. Ceballos Benavides, M. A. Duarte-Mermoud, L. B. Martell, Control Error Convergence Using Lyapunov Direct Method Approach for Mixed Fractional Order Model Reference Adaptive Control, Fractal Fract 9:2 (2025) 98. doi: 10.3390/fractalfract9020098.
[19] J. Zou, P. Lin, Multichannel Attention-Based TCN-GRU Network for Remaining Useful Life Prediction of Aero-Engines, Energies 18:8 (2025) 1899. doi: 10.3390/en18081899.
[20] S. Vladov, V. Vysotska, V. Sokurenko, O. Muzychuk, M. Nazarkevych, V. Lytvyn, Neural Network System for Predicting Anomalous Data in Applied Sensor Systems, Applied System Innovation 7:5 (2024) 88. doi: 10.3390/asi7050088.
[21] I. Perova, Y. Bodyanskiy, Adaptive human machine interaction approach for feature selection-extraction task in medical data mining, International Journal of Computing 17:2 (2018) 113–119. doi: 10.47839/ijc.17.2.997.
[22] W. Gao, M. Pan, W. Zhou, F. Lu, J.-Q. Huang, Aero-Engine Modeling and Control Method with Model-Based Deep Reinforcement Learning, Aerospace 10:3 (2023) 209. doi: 10.3390/aerospace10030209.
[23] N. Shakhovska, V. Yakovyna, N. Kryvinska, An improved software defect prediction algorithm using self-organizing maps combined with hierarchical clustering and data preprocessing. Lecture Notes in Computer Science 12391 (2020) 414–424. doi: 10.1007/978-3-030-59003-1_27.
[24] H. Schieber, K. C. Demir, C. Kleinbeck, S. H. Yang, D. Roth, Indoor Synthetic Data Generation: A Systematic Review, Computer Vision and Image Understanding 240 (2024) 103907. doi: 10.1016/j.cviu.2023.103907.
[25] J. Rabcan, V. Levashenko, E. Zaitseva, M. Kvassay, S. Subbotin, Non-destructive diagnostic of aircraft engine blades by Fuzzy Decision Tree, Engineering Structures 197 (2019 109396. doi: 10.1016/j.engstruct.2019.109396.

[26] S. Vladov, Y. Shmelov, R. Yakovliev, M. Petchenko, Modified Neural Network Fault-Tolerant Closed Onboard Helicopters Turboshaft Engines Automatic Control System, CEUR Workshop Proceedings 3387 (2023) 160–179. URL: https://ceur-ws.org/Vol-3387/paper13.pdf

[27] S. Xiang, Y. Qin, J. Luo, H. Pu, and B. Tang, Multicellular LSTM-based deep learning model for aero-engine remaining useful life prediction, Reliability Engineering & System Safety 216 (2021) 107927. doi: 10.1016/j.ress.2021.107927.

[28] L. Shen, Y. Wang, B. Du, H. Yang, H. Fan, Remaining Useful Life Prediction of Aero-Engine Based on Improved GWO and 1DCNN, Machines 13:7 (2025) 583. doi: 10.3390/machines13070583.

[29] H. Guo, Y. Li, C. Liu, Y. Ni, K. Tang, A Deformation Force Monitoring Method for Aero-Engine Casing Machining Based on Deep Autoregressive Network and Kalman Filter, Applied Sciences 12:14 (2022) 7014. doi: 10.3390/app12147014.

[30] Z. Zhao, Y. Sun, J. Zhang, Fault detection and diagnosis for sensor in an aero-engine system. In Proceedings of the 2016 Chinese Control and Decision Conference (CCDC), Yinchuan, China, 31 May 2014 – 02 June 2014, pp. 2977–2982. doi: 10.1109/ccdc.2016.7531492.

[31] S. Cao, H. Zuo, X. Zhao, C. Xia, Real-Time Gas Path Fault Diagnosis for Aeroengines Based on Enhanced State-Space Modeling and State Tracking, Aerospace 12:7 (2025) 588. doi: 10.3390/aerospace12070588.